

MUC5B mobilizes and MUC5AC spatially aligns mucociliary transport on human airway epithelium

Authors

Daniel Song¹, Ethan Iverson², Logan Kaler³, Margaret A. Scull^{2*}, Gregg A. Duncan^{1,3*}

Affiliations

¹Fischell Department of Bioengineering, University of Maryland, College Park, MD 20742.

²Department of Cell Biology & Molecular Genetics, University of Maryland, College Park, MD 20742.

³Biophysics Program, University of Maryland, College Park, MD 20742.

Corresponding authors e-mail: gaduncan@umd.edu; scull@umd.edu

Abstract

Airway mucus acts as a protective barrier and vehicle for clearance of pathogens, providing the lungs with a defense mechanism called mucociliary clearance (MCC). Airway mucus is composed of two mucins, mucin 5B (MUC5B) and 5AC (MUC5AC) that form a hydrogel that enables functional clearance in health. However, abnormalities in mucin expression, specifically increases in MUC5AC is observed in chronic respiratory diseases and leading to defective MCC. Our current understanding of MCC impairment focuses on mucin concentration, while the impact of mucin composition remains unclear. Here, we use MUC5AC/B-knock out (KO) human airway epithelial (HAE) tissue cultures to understand the role and contribution of individual secreted mucins on MCC mechanisms. We find that KO cultures result in impaired or disorganized mucociliary transport demonstrating the importance of each of these mucins to effective MCC and shedding light on a new mechanism of mucin composition-dependent airway clearance.

Introduction

Airway mucus is a complex biological fluid that protects the lung from environmental insults through a process known as mucociliary clearance (MCC). The mucus layer, which coats the airways, protects the underlying epithelium by acting as a physicochemical barrier immobilizing inhaled pathogens and particulates (1, 2). Unlike other mucosal tissues, the airways can dynamically clear mucus through shear forces exerted by the rapid beating of cilia on the epithelium allowing removal of trapped particulates (3, 4). Normal MCC is essential for innate defense and is facilitated by a transportable mucus layer and coordinated ciliary activity (5).

The primary secreted mucins expressed in the lung are mucin 5B (MUC5B) and 5AC (MUC5AC) (6, 7). These mucins are large (~MDa) glycoproteins that have cysteine-rich domains at their N- and C-termini that cross-link and polymerize via disulfide bonds (4, 8). The resulting network acts as a barrier by controlling the transport of nano- and microscale entities through physical and steric interactions while also giving rise to the viscoelastic nature of mucus (9–13). While MUC5B and MUC5AC have a high degree of similarity in amino acid sequence and domain organization, recent evidence shows that MUC5B and MUC5AC differ in assembly and N-terminal organization, with MUC5B mainly forming dimers, and MUC5AC assembling into dimers as well as higher-order oligomers (14, 15). These subtle differences in macromolecular organization impact the functional properties of secreted mucins, such as effectiveness as a barrier and transportability, which have been

48 studied in *in vivo* animal models (16). In Muc5ac/b knockout (KO) mice, Muc5b deficiency
49 leads to impaired mucus transport and pathogen accumulation, while Muc5ac is shown to
50 be dispensable for transport (17, 18). Nonetheless, in health, the two gel-forming mucins
51 form a mucus gel that is optimized for providing proper protection to the airways.

52
53 In health, MUC5B is the predominant mucin, while MUC5AC is expressed at lower levels
54 (6, 7). While the expression of MUC5B and MUC5AC is tightly regulated to ensure efficient
55 MCC, production of MUC5AC is increased in chronic respiratory diseases due to type I and
56 II immune responses, resulting in a mucus gel with abnormal mucin composition (7, 19–
57 21). Elevated MUC5AC in mucus has been identified as the major driver in impairment of
58 MCC and is correlated with enhanced viscoelastic properties, decreased lung function in
59 chronic bronchitis, and significant mucous plugging in fatal asthma (7, 19, 22, 23). However,
60 how MUC5AC, in health, contributes to effective mucus clearance, while driving the
61 formation of stagnant mucus in disease is unknown. As a result, there is growing interest in
62 understanding how these two secreted mucins with similar domain structures but varying
63 functional properties work in concert to enable efficient airway clearance. Moreover, the
64 spatial coordination of transport on airway surfaces has been largely attributed to cilia
65 organization and activity (24). However, the contribution of secreted mucins to tissue-scale
66 alignment in MCC has not been widely considered.

67
68 In our studies, we developed *in vitro* airway epithelial systems deficient for one of the two
69 gel-forming mucins to investigate the role and contribution of MUC5B and MUC5AC on
70 MCC mechanisms. We used an *in vitro* human airway epithelium model to harvest mucus
71 gels composed of single mucins for rheological assessment. Using our cultures, we
72 measured mucociliary transport rates, while also assessing flow orientation in real-time,
73 demonstrating that MUC5B deficiency leads to impaired mucus clearance, whereas
74 MUC5AC deficiency leads to transport that lacks spatial coordination. Accordingly, we
75 observed that that supplementation of KO cultures with the absent mucin could improve
76 these irregular mucociliary transport phenotypes. Taken together, our data demonstrates the
77 functional significance of both mucins for promoting effective MCC in health, while
78 providing insight into the mechanism of composition-dependent MCC impairment.

80 Results

81 *Generation of MUC5B/AC-KO BCI-NS1.1 cultures*

82 We used CRISPR/Cas9-mediated genome editing to generate *in vitro* HAE models
83 genetically deleted for one of the two gel-forming mucins. We designed two single guide
84 (sg)RNAs that target each mucin gene, MUC5B and MUC5AC, at different exons (**Table**
85 **S1**). Earlier exons were targeted to maximize knock-out efficiency, while two sgRNAs were
86 designed to account for potential off-target effects. As our control, we used a sgRNA with
87 no predicted target. The sgRNAs were cloned into a GFP-expressing lentiviral vector that
88 also encodes the Cas9 nuclease. After lentivirus production, we transduced BCI-NS1.1 cells,
89 an immortalized HAE cell line, which has previously been used for manipulating mucin
90 expression (25–27). Subsequently, transduced cells were expanded, and sorted for GFP
91 expression prior to differentiation (**Fig 1A**). Using a T7 endonuclease cleavage assay, we
92 confirmed editing at the correct genomic loci in undifferentiated cells, evidenced by
93 heteroduplex fragments in all KO conditions (**Fig 1B, C**). To verify that lentiviral
94 transduction did not impact normal differentiation of BCI-NS1.1 cultures, we measured the
95 transepithelial electrical resistance (TEER) 28 days into air-liquid interface (ALI) culture
96 and confirmed TEER values that were within reported ranges in all conditions, indicative
97 of cell polarization and differentiation into a pseudostratified epithelium (**Fig S1**) (28).

Using mucus samples collected from apical washes, we confirmed KO expression on western blot analysis demonstrating loss of MUC5B and MUC5AC expression in KO cultures using respective sgRNA (**Fig 1D**). These data also confirmed that mucus secretions from MUC5B-KO cultures are primarily composed of MUC5AC, while secretions from MUC5AC-KO cultures are composed of MUC5B, allowing us to study the native properties of mucus composed of single mucins.

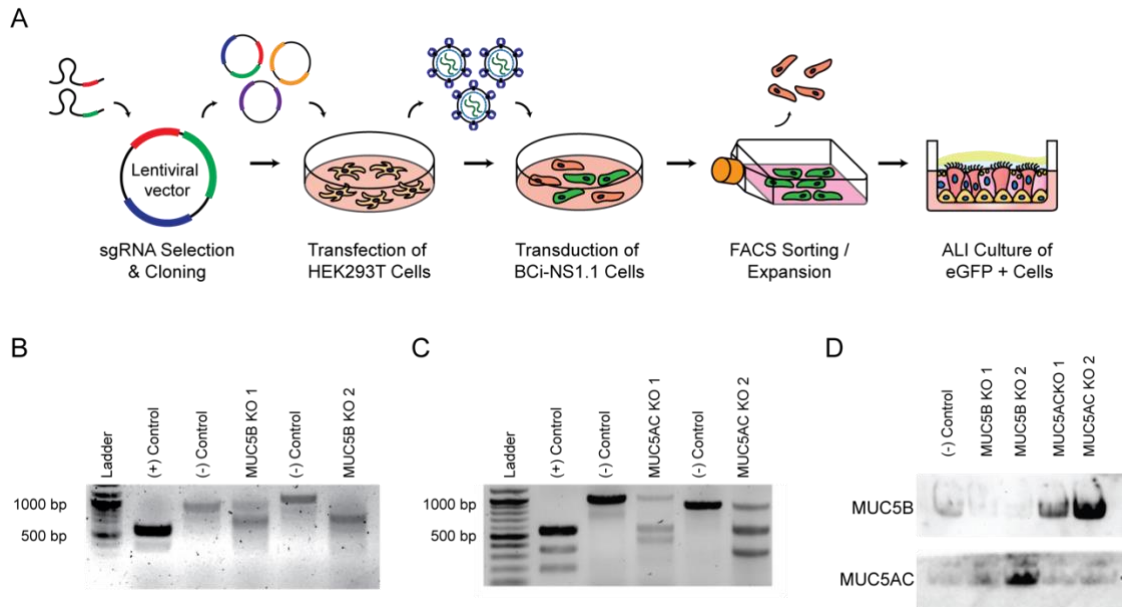


Figure 1. Generation and validation of MUC5B/AC-KO cultures. (A) Overview of MUC5B/MUC5AC gene targeting approach via lentivirus-mediated delivery of sgRNA and CRISPR/Cas9 machinery. (B-C) Validation of on-target editing using T7 endonuclease cleavage assay. Gel images show PCR products amplified from target sites where digested fragments indicate on-site editing. KO1 corresponds to BCI-NS1.1 cells transduced with sgRNA1 and KO2 corresponds to cells transduced with sgRNA2. (+) control corresponds to a control template and primer mix provided with the assay kit. (-) control corresponds to BCI-NS1.1 cells treated with a non-targeting sgRNA. (B) T7 endonuclease cleavage assay using genomic DNA from MUC5B-KO cultures. (C) T7 endonuclease cleavage assay using genomic DNA from MUC5AC-KO cultures. (D) Western blot analysis of mucus samples collected from MUC5B and MUC5AC-KO cultures.

Viscoelasticity of MUC5B and MUC5AC gels

To evaluate the biophysical properties of gels composed of either MUC5B and MUC5AC, we performed macro- and microrheology on pooled mucus samples collected from control and KO cultures. Using macrorheology, we observed elastic dominant properties for all mucus samples ($G' > G''$), confirming a cross-linked polymer network. We also demonstrated that samples exhibited rheological properties in range of previously reported values for mucus collected *in vitro* and *ex vivo* (**Fig 2A**; **Fig S2**) (11–13). While MUC5AC gels resulted in slightly higher mean complex viscosities than other gel types, differences were not statistically significant (**Fig 2B**). We next measured percent solids concentration of each sample as the biophysical properties of a polymer gels are highly sensitive to changes in solids concentration. We found that the solids concentration of pooled mucus samples were within a physiological range (2–4%) (**Fig 2C**) (4, 11). While macrorheological properties have major implications for flow and transport, mucus microstructural network allows mucus to act as a barrier to inhaled material by controlling the diffusion of nano- and microscale entities through physical and adhesive interactions (**Fig 2D**) (4). Therefore, we used particle tracking microrheology (PTM) to assess diffusion of muco-inert nanoparticles

(MIP) through mucus with varying mucin composition to probe mucus microstructure. Results showed that MUC5AC gels had significantly reduced MIP diffusion, as measured by mean square displacement (MSD), and reduced pore size compared to MUC5B gels and mucus collected from control cultures (Fig 2E, F). Comparing the frequency distributions of MIP diffusion, we found that MUC5B gels resulted in MIP diffusion that was similar to mucus obtained from control cultures, whereas MUC5AC gels resulted in a significant reduction in MIP diffusion with multiple peaks indicative of mucus gels with a tighter mesh network and heterogenous structure (Fig 2E, F, G, I). Importantly, we also found that there were no significant differences in macro- and microrheology measurements of MUC5B and MUC5AC gels harvested from cultures with equivalent KO condition (KO1 and KO2) targeted using different sgRNAs.

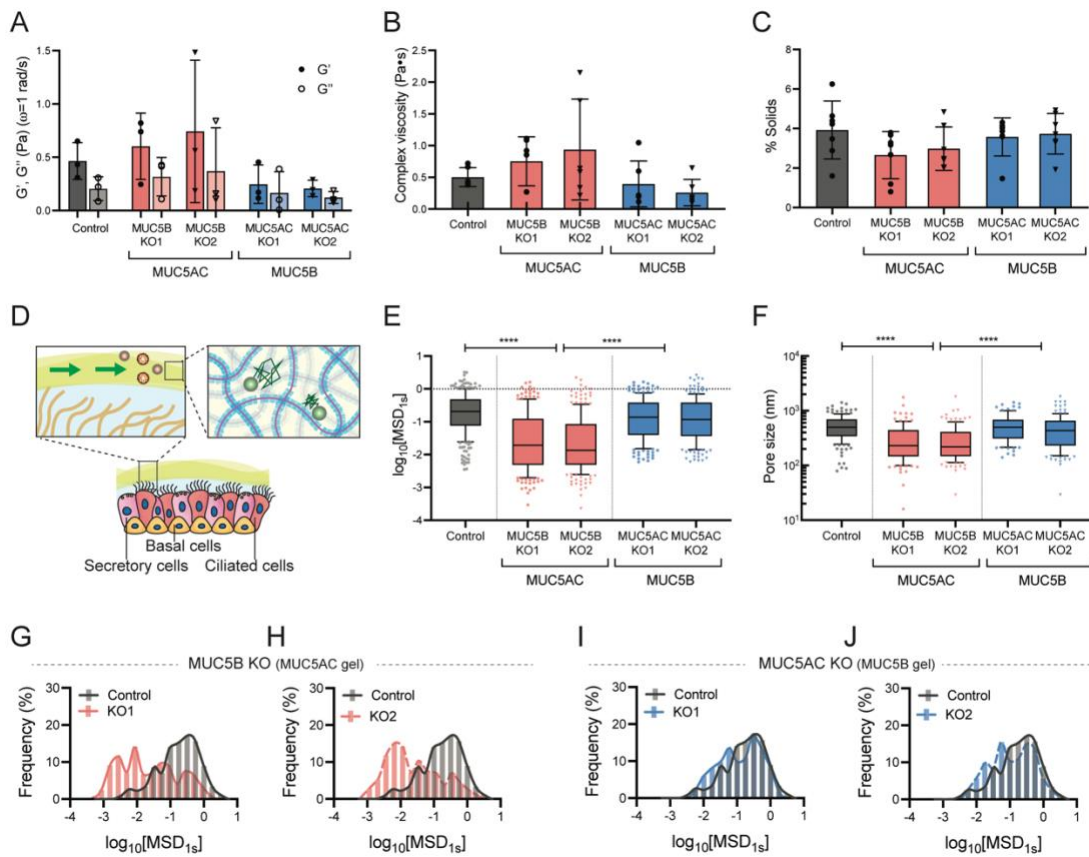
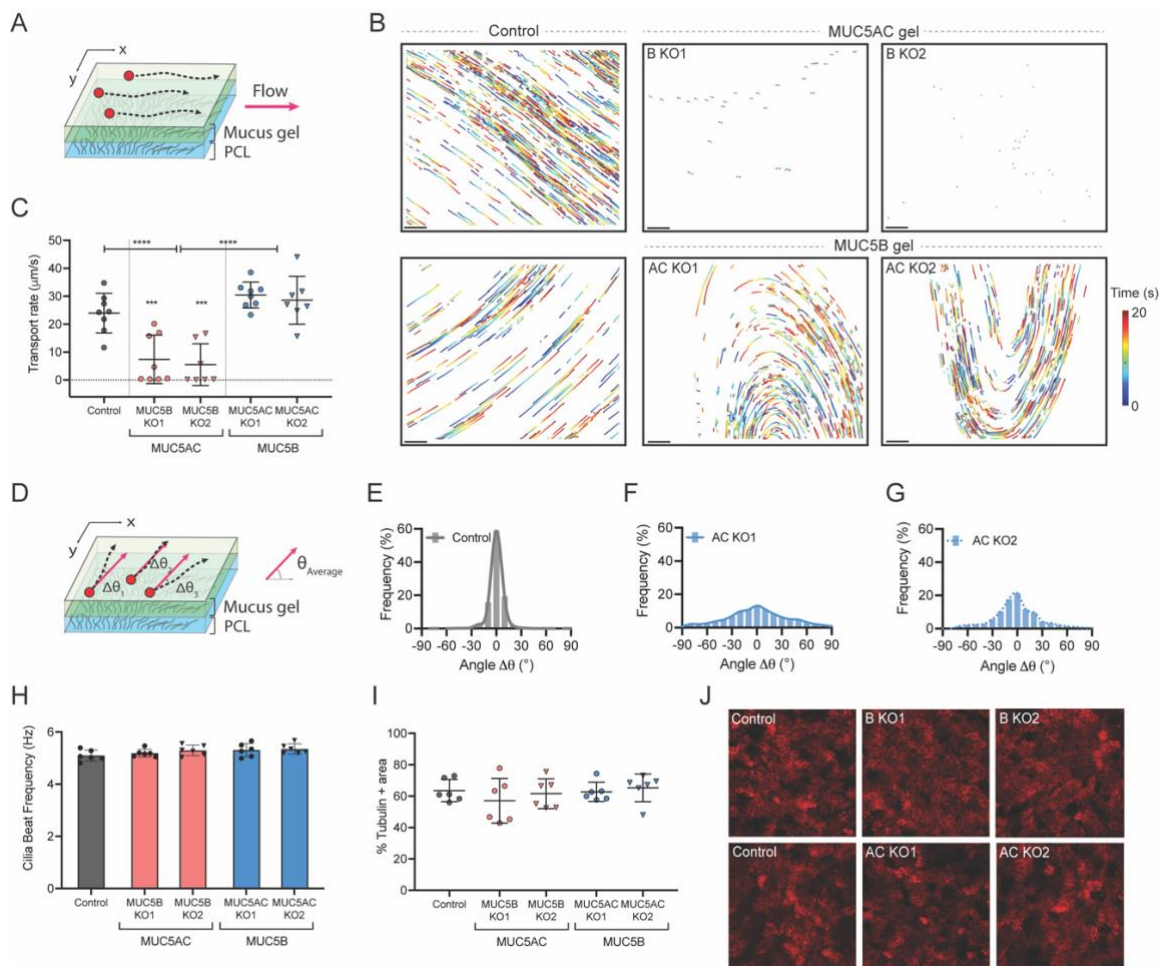


Fig. 2. Viscoelastic properties of mucus produced from MUC5B/AC-KO cultures. (A) Elastic and viscous moduli (G' , G'') at $\omega = 1$ rad/s measured using macrorheology. Moduli show G' -dominant mucus gels. (B) Complex viscosity measured using macrorheology. (C) Concentration of % solids in pooled mucus samples from MUC5B/AC-KO and control cultures. (D) Airway mucus acts as a vehicle of clearance of pathogens, providing the lungs with a robust defense mechanism. Mucus also has a microstructural network that can immobilize diffusing particles. (E) Diffusion of 100 nm PEG-NP in mucus samples from KO cultures as measured by logarithm mean squared displacement (MSD). (F) Estimated pore sizes of mucus samples. (G-J) Frequency distribution of $\log_{10}[\text{MSD}_{1s}]$. Particle distribution in control and (E) MUC5B-KO1, (F) MUC5B-KO2, (G) MUC5AC-KO1, and (H) MUC5AC-KO2 samples.

MUC5B-KO cultures exhibit reduced mucociliary transport and MUC5AC-KO cultures exhibit discoordinated transport

We next examined the mucociliary transport rates of mucus produced from MUC5B or MUC5AC KO cultures to investigate the contribution of each gel-forming mucin on mucociliary clearance. To do so, we deposited 2- μm microspheres onto KO cultures and

163 tracked the movement of particles in real-time (**Fig 3A**). We observed that movement of
 164 microspheres on MUC5B-KO cultures were significantly reduced compared to the non-
 165 targeted control cultures. While functional transport was maintained in MUC5AC-KO
 166 cultures, we observed loss of unidirectional flow (**Fig 3B**). Quantifications of microsphere
 167 speed confirmed that MUC5B-KO cultures had significantly reduced transport rates
 168 compared to control and MUC5AC-KO cultures (**Fig 3C**). We next quantified the
 169 directionality of mucus flow on control and MUC5AC-KO cultures by measuring the angle,
 170 $\Delta\theta$, which was calculated by measuring the angle between individual microsphere trajectory
 171 and ensemble average flow direction ($\theta_{Average}$) (**Fig 3D**). We found that control cultures
 172 resulted in an overall alignment of flow direction, where 95% of the microspheres moved
 173 within 10° to -10° of overall flow (**Fig. 3E**). However, MUC5AC-KO cultures resulted an
 174 irregular flow pattern that resembled circular swirls, where only 35-50% of microspheres
 175 aligned with the ensemble average flow direction (**Fig 3F,G**). We confirmed that these
 176 differences in transport rate and directionality of mucus flow were not likely the result of
 177 changes in the periciliary layer properties by confirming normal cilia beat frequency and
 178 normal cilia expression as demonstrated in +tubulin % area (**Fig 3H-J, Fig S3**).
 179

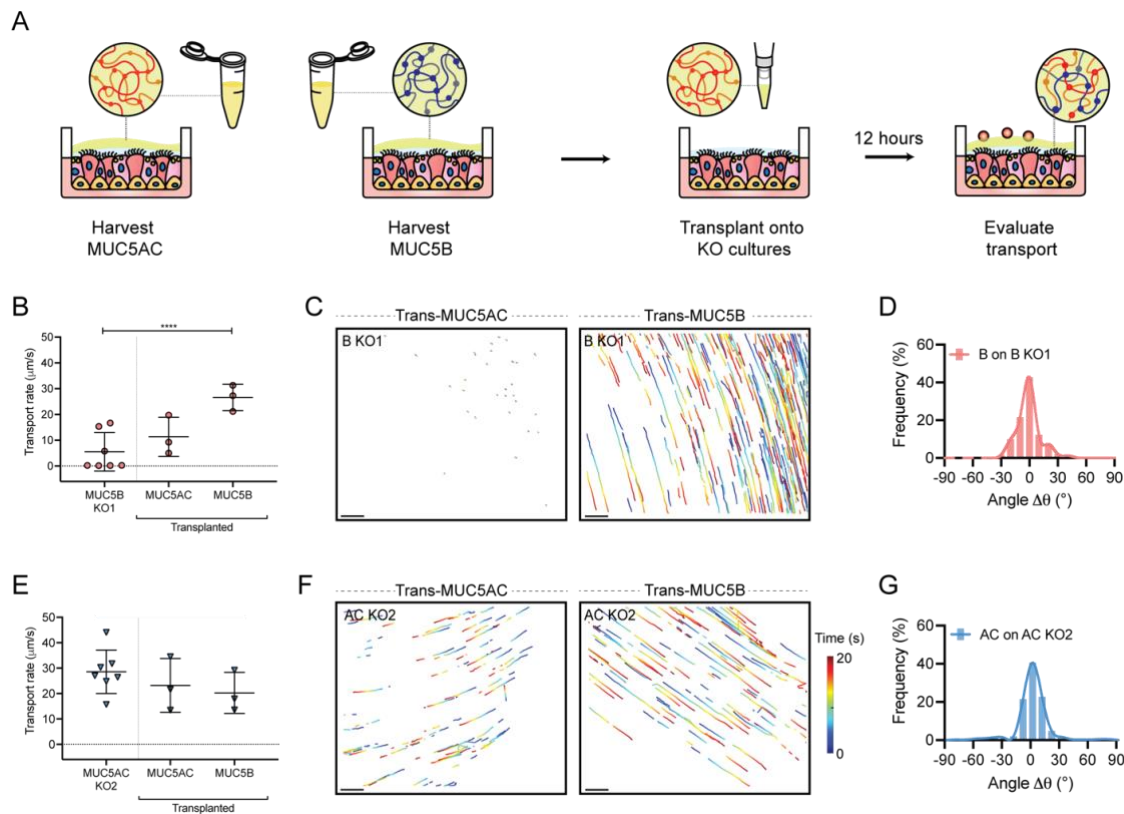


180
 181 **Figure 3. Mucociliary clearance dynamics of MUC5B/AC-KO cultures.** (A) Mucociliary
 182 transport rate is measured by apically applying 2- μm microspheres to cultures and measuring
 183 particle displacement over time. (B) Representative trajectory images of microspheres over time.
 184 Trajectories show 20 s of motion with a color scale that indicates elapsed. Scale bar = 100 μm . (C)
 185 Mucociliary transport rates of MUC5B/AC KO cultures. (D) Trajectory angle, $\Delta\theta$, was calculated
 186 by measuring the angle between and the overall flow direction ($\theta_{Average}$) and instantaneous individual
 187 microsphere trajectory. $\theta_{Average}$ was set to 0° . (E-G) Frequency distribution of $\Delta\theta$. (E) Control (F)
 188 MUC5AC-KO1 (G) MUC5AC-KO2. (H) Cilia beat frequencies of MUC5B/AC KO cultures. (I)

189 Quantification of +tubulin % area. **(J)** Representative image of cilia expression of MUC5B/AC-KO
 190 cultures by immunostaining of acetylated alpha tubulin.

191
 192 *Transplanting exogenous mucus rescues impaired clearance*

193 Our previous data showing abnormal transport resulting from loss of one of the two mucins
 194 led us to hypothesize that supplementing KO cultures with the absent mucin could restore
 195 stalled and/or irregular mucociliary transport phenotypes. To test this, we transplanted
 196 exogenous MUC5B and MUC5AC gels onto KO cultures and tracked the movement of
 197 microspheres on the cultures after equilibration (**Fig 4A**). We chose MUC5B-KO1 and
 198 MUC5AC-KO2 as representative cultures for transplantation experiments. We found that
 199 transplantation of MUC5B onto MUC5B-KO cultures resulted in a significant increase in
 200 transport rates, while also resulting in unidirectional flow (**Fig 4B-D**). However,
 201 transplantation of MUC5AC gels onto their native MUC5B-KO cultures did not result in a
 202 significant change in transport rate. Interestingly, the addition of either MUC5B or
 203 MUC5AC gels onto MUC5AC-KO cultures did not result in any significant change to
 204 transport rates (**Fig. 4E**) but resulted in improved directionality as shown in the trajectory
 205 images (**Fig 4F,G**).



207
 208 **Figure 4. Mucociliary clearance dynamics of transplanted mucus on MUC5B/AC-KO cultures.**

209 **(A)** Exogenous mucus collected from KO cultures was transplanted onto KO cultures to supplement
 210 KO cultures deficient mucin. **(B)** Mucociliary transport rates of transplanted gels on B-KO culture
 211 (MUC5B-KO1 was used). **(C)** Representative trajectory images of microspheres trajectories on
 212 transplanted mucus on B-KO cultures. Scale bar = 100 µm. **(D)** Frequency distribution of $\Delta\theta$,
 213 demonstrating directional flow. **(E)** Mucociliary transport rates of transplanted gels on AC-KO
 214 culture (MUC5AC-KO2 was used). **(F)** Representative trajectory images of microspheres
 215 trajectories on transplanted mucus on AC-KO cultures. Scale bar = 100 µm. **(G)** Frequency
 216 distribution of $\Delta\theta$, demonstrating directional flow.

Discussion

In these studies, we report *in vitro* HAE models that are genetically depleted for one of the two gel-forming mucins expressed in airway mucus to understand their role and overall contribution in mucociliary clearance mechanisms. We targeted MUC5B and MUC5AC genes in the BCi-NS1.1 human airway basal cell line and demonstrated successful editing at targeted genomic loci in undifferentiated cultures, while confirming KO expression in pooled mucus washings post-differentiation. MUC5B-KO cultures produced gels composed primarily of MUC5AC, while MUC5AC-KO cultures produced MUC5B gels, which allowed us to study each mucin independently. We note that our western blot analysis indicates that KO cultures produce slightly elevated levels of respective mucins compared to control cultures, while overall percent solids and protein concentration are conserved. These results may indicate that MUC5B and MUC5AC secretion is hydrodynamically controlled, regardless of mucin type. However, the pathways that regulate secretion of each mucin after KO will need to be explored in future studies.

Using our KO cultures, we assessed the biophysical properties of mucus samples with varying mucin composition. Our results indicate that gels composed of MUC5AC have altered microstructural properties compared to MUC5B gels, where pore size is significantly reduced and heterogenous. These results are consistent with recent findings that show that MUC5AC secreted from CALU3 cells form tight networks with high degrees of branching, while MUC5B organizes in linear strands (15). The smaller pore size in MUC5AC gels have implications for their functional role as a protective gel against pathological and chemical insults to the airway. In past work, MUC5AC has been shown to protect against viral respiratory pathogens such as influenza and prevent parasite infiltration (21, 29, 30). We also observed major differences in transportability of gels composed of different mucin types. MUC5AC gels produced from MUC5B-KO cultures were poorly cleared, while MUC5B gels from MUC5AC-KO cultures were more easily transported. These data are consistent with previous mouse models that showed that Muc5b-KO in mice, but not Muc5ac-KO, resulted in impaired mucociliary clearance and mucus accumulation in the airways (17). Furthermore, in humans, new evidence has shown that congenital absence of MUC5B results in impaired mucus clearance (31). This may be due in part to macromolecular organization of mucins, where MUC5B forms linear gels that can be easily transported via ciliary activity, while MUC5AC forms a tighter gel, which increases friction between gel surfaces, resulting in poor clearance (3, 15). While bulk rheological properties are known to impact transport properties of the mucus gels, our data showed no resolvable differences in viscosities between gels of varying mucin types (4). Previous studies have predicted MUC5AC to form more elastic gels than MUC5B and we note that MUC5AC gels had higher complex viscosities compared to MUC5B gels, despite having lower percent solids concentration (15). We expect solids concentration-matched MUC5B and MUC5AC gels would possess even greater differences in their viscoelastic properties and this will be explored in subsequent work.

Despite functional transport of MUC5B gels on MUC5AC-KO cultures, we observed that MUC5AC deficiency led to poor directionality with local swirls, while control cultures that expressed both mucins showed global order. These transport patterns have been previously observed in HAE *in vitro* models and attributed to hydrodynamic active coupling between mucus and cilia, where changes in mucus properties and cilia density can alter the overall orientation of mucus flow (32, 33). While the role of MUC5AC in mucociliary transport has been largely overlooked, our data suggests that MUC5AC-enhanced mucus viscoelasticity plays a significant role in hydrodynamic coupling between the mucus and

269 periciliary layers, driving long-range transport and effective clearance. This can also be
270 explained by our transplantation experiments with exogenous mucus, where we
271 demonstrated that supplementation of KO cultures with the absent mucin can rescue and
272 improve irregular transport phenotypes. We note supplementation of MUC5B to MUC5B–
273 expressing cultures also improved transport coordination likely by increasing mucin
274 concentration and mucus gel viscoelasticity leading to enhanced hydrodynamic coupling.
275 However overall, these experiments demonstrate the biological importance of both gel-
276 forming mucins, MUC5B and MUC5AC for efficient mucociliary transport in the airways.

277
278 Our current understanding of impaired mucus clearance has primarily focused on the
279 imbalance in osmotic pressure between the mucus and periciliary layer, which results from
280 a dehydrated or hyper-concentrated mucus gel that is not easily cleared (3, 34). However,
281 our findings shed light on the mechanisms of defective mucociliary clearance dictated by
282 mucus composition and independent of concentration. While increased MUC5AC may
283 contribute to protection against inhaled pathogens through physical obstruction,
284 disproportionate increases have been associated with pathogenesis of chronic obstructive
285 lung diseases and airway obstruction (7, 19). Mucous plugs from individuals with fatal
286 asthma show MUC5AC enrichment and localization close to the epithelium. In mice,
287 *Muc5ac* mediates mucous occlusion after allergic stimulation, while *Muc5ac*-KO resulted
288 in significant protection against mucus plugging. Taken together, elevated levels of
289 MUC5AC on the epithelial surface could be a significant contributor to mucus accumulation
290 and airway obstruction due to its poor transportability as demonstrated in our studies.

291
292 In conclusion, our study provides unique insight into the contribution of each gel-forming
293 mucin, MUC5B and MUC5AC on mucociliary clearance mechanisms, demonstrating the
294 significance of each mucin. Our findings suggest secretion of MUC5B and MUC5AC offer
295 a means for the airway epithelium to dynamically control mucus transport velocity and flow
296 alignment. While MUC5AC has been considered to be a potential therapeutic target for
297 allergic asthma (35), we predict that preserving baseline levels of MUC5AC could be
298 important in maintaining flow orientation to facilitate effective removal of pathogens. To
299 resolve MUC5AC–induced MCC dysfunction, ongoing work on mucolytic strategies that
300 target the disulfide bonds in mucus gels for normalizing clearance may prove useful as
301 MUC5AC–enriched gels are likely to be more extensively crosslinked (15, 36). This work
302 also establishes the premise for future development of new precision therapies aimed at
303 restoring an optimal balance of MUC5B and MUC5AC secretion in airway diseases.

304 **Materials and Methods**

305 *CRISPR/Cas9-mediated knockout of MUC5B and MUC5AC*

306 We utilized lentivirus for CRISPR/Cas9-mediated gene targeting of MUC5B and MUC5AC in BCi-
307 NS1.1 cells, an h-TERT immortalized human airway basal cell line, generously provided by Dr.
308 Ronald Crystal, which their group established and characterized in previous work (25). Two single
309 guide (sg) RNAs that target different regions of MUC5B and MUC5AC were selected based on
310 favorable targeting using the Doench and Xu scores. To generate negative control, we designed
311 sgRNA sequences with no matching sequence in the genome (non-targeting control). Selected
312 gRNAs were cloned into a GFP-expressing lentiviral vector, pLENTICRISPRv2-GFP, (a gift from
313 Dr. Feng Zhang (Addgene plasmid #52961; <http://n2t.net/addgene:52961>; RRID:Addgene_52961)),
314 which also encodes Cas9 nuclease. Lentiviral stalks were generated by co-transfecting
315 plentiCRISPRv2, pCMV-VSV-G (a gift from Dr. Bob Weinberg (Addgene plasmid #8454;
316 <http://n2t.net/addgene:8454>; RRID:Addgene_8454), and psPAX2 (a gift from Dr. Didier Trono
317 (Addgene plasmid #12260; <http://n2t.net/addgene:12260>; RRID:Addgene_12260)) into HEK293T
318 cells with jetPrime (Polyplus) in cell media, DMEM (Gibco) supplemented with 10% fetal bovine
319 serum using manufacturer's protocol. BCi-NS1.1 cells were transduced at 40-60% confluence using
320

321 harvested lentiviruses in media with a final concentration of 20 mM HEPES (Gibco) and 4 $\mu\text{g} / \text{mL}$
322 Polybrene (American Bio). BCi-NS1.1 cells were then centrifuged (1,000 g for one hour at 37°C)
323 and incubated at 37°C overnight. At 60-80% confluence cells were passaged and expanded and
324 sorted for eGFP expression.

325 *T7 endonuclease cleavage assay*

326 DNA from transduced, sorted (eGFP+) cells was extracted using QuickExtract DNA Extraction
327 Solution (Lucigen). EnGen Mutation Detection Kit (New England BioLabs) was used for
328 amplification of target DNA, heteroduplex formation, and heteroduplex digestion, using
329 manufacturer's protocol. Final DNA products were separated and visualized in a 1% agarose gel
330 through gel electrophoresis.
331

332 *Cell Culture*

333 Transduced and sorted (eGFP+) BCi-NS1.1 cells were seeded on plastic at ~ 3000 cells/cm² in
334 PneumaCult-Ex Plus media (StemCell) and incubated at 37°C, 5% CO₂. Once cells reached 70-80%
335 confluency, they were dissociated using 0.05% trypsin ethylenediaminetetraacetic acid (EDTA) for
336 5 minutes at 37°C. To establish well-differentiated human airway epithelial (HAE) tissues cultures
337 grown at an air-liquid interface (ALI), BCi-NS1.1 cells were seeded on 12 mm diameter transwell
338 inserts (Corning Costar) coated with 50 $\mu\text{g}/\text{mL}$ type 1-collagen from rat-tail (Corning) at $\sim 10,000$
339 cells/cm². Expansion media, PneumaCult-Ex Plus, was used to feed cells in both the apical and
340 basolateral compartments until 100% confluency. After reaching confluency, the apical media was
341 removed to transition from submerged to ALI culture and the basolateral media was replaced with
342 PneumaCult-ALI (StemCell). All cells were grown for 28 days to reach differentiation with media
343 exchanged every other day. Transepithelial electrical resistance (TEER) was quantified cultures
344 using the Millicell Electrical Resistance System ERS-2 Volt-Ohm Meter (Millipore).
345

346 *Mucus collection*

347 Once fully differentiated, mucus was allowed to accumulate prior to collection every 3-4 days.
348 Mucus samples were harvested by washing apical compartments with PBS for 30 minutes at 37°C.
349 After 30 minutes incubation, the solution of mucus and PBS was collected (11, 13). Samples were
350 loaded into Amicon Ultra 100 kDa filters (Millipore-Sigma) and centrifuged at 14,000 $\times g$ for 20
351 minutes to remove excess PBS for mucin isolation. Mucus samples were stored at -80 °C for long-
352 term storage (> 2 weeks) or stored at 4 °C (26). Pooled mucus samples were used for western blot
353 analysis, solids concentration analysis, biophysical characterization, and transport experiments.
354

355 *Western blot analysis*

356 Mucus samples from BCi-NS1.1 cell washings were used for western blot analysis. Protein
357 concentration of samples was quantified using BCA assay (Pierce, Thermo Scientific) and equal
358 amounts (10 μg) were loaded into each lane and run on a 4-20% Tris-Glycine gel (Novex,
359 Invitrogen) under reducing conditions. Proteins were transferred to a polyvinylidene fluoride
360 (PVDF) membrane (GE Healthcare) and blocked with 5% (w/v) fat free milk protein in tris-buffered
361 saline, 0.1% Tween (TBS-T) at room temperature. Primary antibody incubation was over night at
362 4°C in 5% (w/v) fat free milk protein. The primary antibodies that were used were mouse anti-
363 MU5AC (1:1,000; cat. no. ab3649; Abcam) and rabbit anti-MUC5B UNC414 (1:1,000), generously
364 gifted by Dr. Camille Ehre. After washing in TBS-T, membranes were probed with secondary
365 antibodies for one hour at room temperature in blocking buffer. The secondary antibodies that were
366 used were anti-mouse IgGk-HRP (sc-516102, Santa Cruz, 1:10,000), anti-rabbit-HRP
367 (32460, Invitrogen, 1:10,000). Imaging was performed with chemiluminescent SuperSignal Dura
368 reagent (Thermo Scientific) on an iBright 1500 (Thermo Fisher).
369

370 *Mucus solids concentration*

371 We measured solids concentrations of mucus samples by aliquoting 50 μL of mucus on weighing
372 paper of known mass and recording the combined mass of the mucus sample and paper. The samples
373 were then placed on a heat plate at 60°C for 4-5 hours. The final mass of the dried sample and
374 weighing paper was recorded and used to calculate % solids concentration.
375

376
377
378
379
380
381
382
383
384
385
386
387
388
389
390
391
392
393
394
395
396
397
398
399
400
401
402
403
404
405
406
407
408
409
410
411
412
413
414
415
416
417
418
419
420
421
422
423
424
425
426
427
428
429

Bulk rheology

Dynamic rheological measurements of mucus gels harvested and pooled from ALI cultures were performed using the ARES G2 rheometer (TA Instruments) with a 40-mm diameter 2° cone and plate geometry at 25°C. To determine the linear viscoelastic region of the fully formed gel, a strain sweep measurement was collected from 0.1-10% strain at a frequency of 1 rad s⁻¹. To determine the elastic modulus, $G'(\omega)$, and viscous modulus, $G''(\omega)$, a frequency sweep measurement was conducted within the linear viscoelastic region of the gel, at 1% strain amplitude and angular frequencies from 0.1 to 10 rad s⁻¹.

Particle Tracking Microrheology (PTM)

Carboxylate-modified, fluorescent polystyrene nanoparticles (PS-COOH; Life Technologies) with a diameter of 100 nm were coated with a high surface density of polyethylene glycol (PEG) via a carboxyl-amine linkage using 5-kDa methoxy PEG-amine (Creative PEGWorks) as previously reported (9, 37). Particle size and zeta potential was measured in 10 mM NaCl at pH 7 using a NanoBrook Omni (Brookhaven Instruments). We measured diameters of 122 nm and zeta potentials of -0.54 ± 1.16 for 100 nm PEG-coated PS nanoparticles, respectively. The diffusion of the PEG-coated nanoparticles (PEG-NP) in mucus gels was measured using fluorescence video microscopy. Twenty five μL of mucus was added to the chamber along with 1 μL of $\sim 0.002\%$ w/v suspension of PEG-NP 30 minutes prior to particle tracking microrheology (PTM) experiments. Videos were collected using a Zeiss 800 LSM microscope with a 63x water-immersion objective and an AxioCam 702 camera (Zeiss) at a frame rate of 33 Hz for 10 seconds at room temperature. For each sample, at least 3 high-speed videos were recorded. The particle tracking analysis was performed using a previously developed image processing algorithm (37, 38). Mean squared displacement (MSD) as a function of time lag (τ) was calculated as

$$\langle \Delta r^2(\tau) \rangle = \langle (x^2 + y^2) \rangle \quad (1)$$

for each particle. Using the generalized Stokes-Einstein relation, measured MSD values were used to compute viscoelastic properties of the hydrogels. The Laplace transform of $\langle \Delta r^2(\tau) \rangle$, $\langle \Delta r^2(s) \rangle$, is related to viscoelastic spectrum $\tilde{G}(s)$ using the equation

$$\tilde{G}(s) = 2k_B T / [\pi a s \langle \Delta r^2(s) \rangle] \quad (2)$$

where $k_B T$ is the thermal energy, a is the particle radius, s is the complex Laplace frequency. The complex modulus can be calculated as

$$G^*(\omega) = G'(\omega) + G''(i\omega) \quad (3)$$

with $i\omega$ being substituted for s , where i is a complex number and ω is frequency. Hydrogel network pore size, ξ , is estimated based on G' using the equation,

$$\xi \approx (k_B T / G')^{1/3} \quad (4)$$

Mucociliary transport and ciliary beat frequency

For measurement of mucociliary transport rate, a 4 μL suspension of 2 μm red-fluorescent polystyrene microspheres (Sigma-Aldrich; 1:1000 dilution in PBS) was apically applied to native mucus, which was allowed to accumulate for 1-2 days prior to analysis. After equilibration overnight, videos of three regions were recorded at 10x magnification using a Zeiss 800 LSM microscope. Images were collected at a frame rate of 0.5 Hz for 20 seconds on the plane of the mucus gel. The microsphere tracking data analysis is based on an image processing algorithm that was custom written in MATLAB (26, 39). Briefly, the analysis software computes the xy-plane trajectories of each fluorescent microsphere in each frame. Using the trajectory data, displacement of microspheres was computed, and transport rate was calculated by dividing the distance traveled by total elapsed time. In order to measure ciliary beat frequency (CBF), 10 second videos at a frame rate of 20 Hz were recorded at 20x magnification in ≥ 3 randomly selected regions of each BCi-NS1.1 culture using brightfield. Using a custom written algorithm in MATLAB, the number of local pixel intensity maxima were counted, which indicates beating of cilia. Beat frequency was determined by dividing the number of beats over the total elapsed time.

Immunostaining

BCi-NS1.1 cultures were fixed using 4% paraformaldehyde for 30 minutes at room temperature. Inserts were washed with PBS and blocked with 5% bovine serum albumin (BSA) in PBS and 0.01% triton X-100 for 1 hour at room temperature. After blocking, fixed cultures were incubated overnight at 4°C with AlexaFluor conjugated antibodies in 5% BSA in PBS. The antibodies that were used were anti-acetylated alpha tubulin AlexaFluor 647 (cilia marker, clone 6-11B-1, sc23950, Santa Cruz, 1:2000) and ZO-1 monoclonal antibody AlexaFluor 488 (tight junction marker, ZO1-1A12, Invitrogen, 1:2000). Inserts were washed with PBS three times and imaged at 63x magnification using a Zeiss 800 LSM microscope (Zeiss). Quantification of % tubulin positive area was performed in FIJI using the automated thresholding function.

Mucus Transplantation

Reconstituted mucus samples from KO culture washings were used for transplantation studies. 20 µL of mucus was applied to the apical surface of ALI cultures that had been washed with PBS for 30 minutes (26, 40). 2 µm red-fluorescent polystyrene microspheres were applied immediately after transplantation of exogenous mucus. Mucociliary transport rates were measured after equilibration overnight as described in the methods above .

Statistical Analysis

All graphing and statistical analyses were performed using GraphPad Prism 8 (GraphPad Software). Two-group comparisons were performed using 2-tailed Student's *t*-test (normally distributed data) or Mann-Whitney *U* test. For comparisons between groups, one-way analysis of variance (ANOVA) followed by a Tukey *post hoc* correction was performed. Kruskal-Wallis with Dunn's correction was used for comparison of multiple groups with non-Gaussian distributions. Bar graphs show mean and standard deviation and box and whiskers plots show median. Differences were considered statistically different at the level of $p < 0.05$.

References

1. J. V. Fahy, B. F. Dickey, Airway Mucus Function and Dysfunction. *N. Engl. J. Med.* **363**, 2233–2247 (2010).
2. M. Kesimer, C. Ehre, K. A. Burns, C. W. Davis, J. K. Sheehan, R. J. Pickles, Molecular organization of the mucins and glycocalyx underlying mucus transport over mucosal surfaces of the airways. *Mucosal Immunol.* **6**, 379–392 (2013).
3. B. Button, L.-H. Cai, C. Ehre, M. Kesimer, D. B. Hill, J. K. Sheehan, R. C. Boucher, M. Rubinstein, A Periciliary Brush Promotes the Lung Health by Separating the Mucus Layer from Airway Epithelia. *Science (80-.)*. **337**, 937–941 (2012).
4. D. Song, D. Cahn, G. A. Duncan, Mucin Biopolymers and Their Barrier Function at Airway Surfaces. *Langmuir* (2020), doi:10.1021/acs.langmuir.0c02410.
5. M.-K. Khelloufi, E. Loiseau, M. Jaeger, N. Molinari, P. Chanez, D. Gras, A. Viallat, Spatiotemporal organization of cilia drives multiscale mucus swirls in model human bronchial epithelium. *Sci. Rep.* **8**, 2447 (2018).
6. M. E. Lachowicz-Scroggins, S. Yuan, S. C. Kerr, E. M. Dunican, M. Yu, S. D. Carrington, J. V. Fahy, Abnormalities in MUC5AC and MUC5B protein in airway mucus in asthma. *Am. J. Respir. Crit. Care Med.* **194** (2016), pp. 1296–1299.
7. M. Kesimer, A. A. Ford, A. Ceppe, G. Radicioni, R. Cao, C. W. Davis, C. M. Doerschuk, N. E. Alexis, W. H. Anderson, A. G. Henderson, R. G. Barr, E. R. Bleecker, S. A. Christenson, C. B. Cooper, M. K. Han, N. N. Hansel, A. T. Hastie, E. A. Hoffman, R. E. Kanner, F. Martinez, R. Paine, P. G. Woodruff, W. K. O'Neal, R. C. Boucher, Airway Mucin Concentration as a Marker of Chronic Bronchitis. *N. Engl. J. Med.* **377**, 911–922 (2017).
8. D. J. Thornton, K. Rousseau, M. A. McGuckin, Structure and Function of the Polymeric Mucins in Airways Mucus. *Annu. Rev. Physiol.* **70**, 459–486 (2008).
9. B. S. Schuster, J. S. Suk, G. F. Woodworth, J. Hanes, Nanoparticle diffusion in respiratory

- 482 mucus from humans without lung disease. *Biomaterials*. **34**, 3439–3446 (2013).
- 483 10. G. A. Duncan, J. Jung, A. Joseph, A. L. Thaxton, N. E. West, M. P. Boyle, J. Hanes, J. S.
- 484 Suk, Microstructural alterations of sputum in cystic fibrosis lung disease. *JCI insight*. **1**,
- 485 e88198 (2016).
- 486 11. D. B. Hill, P. A. Vasquez, J. Mellnik, S. A. McKinley, A. Vose, F. Mu, A. G. Henderson,
- 487 S. H. Donaldson, N. E. Alexis, R. C. Boucher, M. G. Forest, A biophysical basis for mucus
- 488 solids concentration as a candidate biomarker for airways disease. *PLoS One*. **9**, e87681
- 489 (2014).
- 490 12. A. L. Innes, S. D. Carrington, D. J. Thornton, S. Kirkham, K. Rousseau, R. H. Dougherty,
- 491 W. W. Raymond, G. H. Caughey, S. J. Muller, J. V. Fahy, Ex vivo sputum analysis reveals
- 492 impairment of protease-dependent mucus degradation by plasma proteins in acute asthma.
- 493 *Am. J. Respir. Crit. Care Med*. **180**, 203–210 (2009).
- 494 13. M. R. Markovetz, D. B. Subramani, W. J. Kissner, C. B. Morrison, I. C. Garbarine, A.
- 495 Ghio, K. A. Ramsey, H. Arora, P. Kumar, D. B. Nix, T. Kumagai, T. M. Krunkosky, D. C.
- 496 Krause, G. Radicioni, N. E. Alexis, M. Kesimer, M. Tiemeyer, R. C. Boucher, C. Ehre, D.
- 497 B. Hill, Endotracheal tube mucus as a source of airway mucus for rheological study. *Am. J.*
- 498 *Physiol. Lung Cell. Mol. Physiol*. **317**, L498–L509 (2019).
- 499 14. L. Bonser, D. Erle, Airway Mucus and Asthma: The Role of MUC5AC and MUC5B. *J.*
- 500 *Clin. Med*. **6**, 112 (2017).
- 501 15. J. Carpenter, Y. Wang, R. Gupta, Y. Li, P. Haridass, D. B. Subramani, B. Reidel, L.
- 502 Morton, C. Ridley, W. K. O’Neal, M. P. Buisine, C. Ehre, D. J. Thornton, M. Kesimer,
- 503 Assembly and organization of the N-terminal region of mucin MUC5AC: Indications for
- 504 structural and functional distinction from MUC5B. *Proc. Natl. Acad. Sci. U. S. A.* **118**
- 505 (2021), doi:10.1073/PNAS.2104490118/-/DCSUPPLEMENTAL.
- 506 16. C. E. Wagner, K. M. Wheeler, K. Ribbeck, Mucins and Their Role in Shaping the
- 507 Functions of Mucus Barriers. *Annu. Rev. Cell Dev. Biol.* **34**, 189–215 (2018).
- 508 17. M. G. Roy, A. Livraghi-Butrico, A. A. Fletcher, M. M. McElwee, S. E. Evans, R. M.
- 509 Boerner, S. N. Alexander, L. K. Bellinghausen, A. S. Song, Y. M. Petrova, M. J. Tuvim, R.
- 510 Adachi, I. Romo, A. S. Bordt, M. G. Bowden, J. H. Sisson, P. G. Woodruff, D. J. Thornton,
- 511 K. Rousseau, M. M. De La Garza, S. J. Moghaddam, H. Karmouty-Quintana, M. R.
- 512 Blackburn, S. M. Drouin, C. W. Davis, K. A. Terrell, B. R. Grubb, W. K. O’Neal, S. C.
- 513 Flores, A. Cota-Gomez, C. A. Lozupone, J. M. Donnelly, A. M. Watson, C. E. Hennessy,
- 514 R. C. Keith, I. V. Yang, L. Barthel, P. M. Henson, W. J. Janssen, D. A. Schwartz, R. C.
- 515 Boucher, B. F. Dickey, C. M. Evans, Muc5b is required for airway defence. *Nature*. **505**,
- 516 412–416 (2014).
- 517 18. C. M. Evans, D. S. Raclawska, F. Ttofali, D. R. Liptzin, A. A. Fletcher, D. N. Harper, M.
- 518 A. McGing, M. M. McElwee, O. W. Williams, E. Sanchez, M. G. Roy, K. N. Kindrachuk,
- 519 T. A. Wynn, H. K. Eltzschig, M. R. Blackburn, M. J. Tuvim, W. J. Janssen, D. A.
- 520 Schwartz, B. F. Dickey, The polymeric mucin Muc5ac is required for allergic airway
- 521 hyperreactivity. *Nat. Commun.* **6**, 6281 (2015).
- 522 19. L. R. Bonser, L. Zlock, W. Finkbeiner, D. J. Erle, Epithelial tethering of MUC5AC-rich
- 523 mucus impairs mucociliary transport in asthma. *J. Clin. Invest.* **126**, 2367–2371 (2016).
- 524 20. E. Doz, N. Noulin, E. Boichot, I. Guénon, L. Fick, M. Le Bert, V. Lagente, B. Ryffel, B.
- 525 Schnyder, V. F. J. Quesniaux, I. Couillin, Cigarette smoke-induced pulmonary
- 526 inflammation is TLR4/MyD88 and IL-1R1/MyD88 signaling dependent. *J. Immunol.* **180**,
- 527 1169–1178 (2008).
- 528 21. D. Rajan, E. L. O’Keefe, C. Travers, C. McCracken, S. Geoghegan, M. T. Caballero, P. L.
- 529 Acosta, F. Polack, L. J. Anderson, MUC5AC Levels Associated With Respiratory
- 530 Syncytial Virus Disease Severity. *Clin. Infect. Dis.* **67**, 1441–1444 (2018).
- 531 22. E. M. Dunican, B. M. Elicker, D. S. Gierada, S. K. Nagle, M. L. Schiebler, J. D. Newell,

- 532 W. W. Raymond, M. E. Lachowicz-Scroggins, S. Di Maio, E. A. Hoffman, M. Castro, S.
533 B. Fain, N. N. Jarjour, E. Israel, B. D. Levy, S. C. Erzurum, S. E. Wenzel, D. A. Meyers, E.
534 R. Bleecker, B. R. Phillips, D. T. Mauger, E. D. Gordon, P. G. Woodruff, M. C. Peters, J.
535 V. Fahy, P. Noel, R. Smith, Mucus plugs in patients with asthma linked to eosinophilia and
536 airflow obstruction. *J. Clin. Invest.* **128**, 997–1009 (2018).
- 537 23. D. S. Raclawska, F. Ttofali, A. A. Fletcher, D. N. Harper, B. S. Bochner, W. J. Janssen, C.
538 M. Evans, Mucins and Their Sugars. Critical Mediators of Hyperreactivity and
539 Inflammation. *Ann. Am. Thorac. Soc.* **13 Suppl 1**, S98-9 (2016).
- 540 24. G. R. Ramirez-San Juan, A. J. T. M. Mathijssen, M. He, L. Jan, W. Marshall, M. Prakash,
541 Multi-scale spatial heterogeneity enhances particle clearance in airway ciliary arrays. *Nat.*
542 *Phys.* **2020 169**, **16**, 958–964 (2020).
- 543 25. M. S. Walters, K. Gomi, B. Ashbridge, M. A. S. Moore, V. Arbelaez, J. Heldrich, B. Sen
544 Ding, S. Rafii, M. R. Staudt, R. G. Crystal, Generation of a human airway epithelium
545 derived basal cell line with multipotent differentiation capacity. *Respir. Res.* **14**, 135
546 (2013).
- 547 26. D. Song, E. Iverson, L. Kaler, S. Bader, M. A. Scull, G. A. Duncan, Modeling Airway
548 Dysfunction in Asthma Using Synthetic Mucus Biomaterials. *ACS Biomater. Sci. Eng.* **7**,
549 2723–2733 (2021).
- 550 27. A. T. Reid, K. S. Nichol, P. C. Veerati, F. Moheimani, A. Kicic, S. M. Stick, N. W.
551 Bartlett, C. L. Grainge, P. A. B. Wark, P. M. Hansbro, D. A. Knight, Blocking notch3
552 signaling abolishes MUC5AC production in airway epithelial cells from individuals with
553 asthma. *Am. J. Respir. Cell Mol. Biol.* **62**, 513–523 (2020).
- 554 28. H. W. Chu, C. Rios, C. Huang, A. Wesolowska-Andersen, E. G. Burchard, B. P.
555 O’Connor, T. E. Fingerlin, D. Nichols, S. D. Reynolds, M. A. Seibold, CRISPR-Cas9-
556 mediated gene knockout in primary human airway epithelial cells reveals a
557 proinflammatory role for MUC18. *Gene Ther.* **22**, 822–829 (2015).
- 558 29. C. Ehre, E. N. Worthington, R. M. Liesman, B. R. Grubb, D. Barbier, W. K. O’Neal, J. M.
559 Sallenave, R. J. Pickles, R. C. Boucher, Overexpressing mouse model demonstrates the
560 protective role of Muc5ac in the lungs. *Proc. Natl. Acad. Sci. U. S. A.* **109**, 16528–16533
561 (2012).
- 562 30. S. Z. Hasnain, C. M. Evans, M. Roy, A. L. Gallagher, K. N. Kindrachuk, L. Barron, B. F.
563 Dickey, M. S. Wilson, T. A. Wynn, R. K. Grenicis, D. J. Thornton, Muc5ac: a critical
564 component mediating the rejection of enteric nematodes. *J. Exp. Med.* **208**, 893–900
565 (2011).
- 566 31. G. Costain, Z. Liu, V. Mennella, G. Radicioni, A. N. Goczi, A. Albuлесcu, S. Walker, B.
567 Ngan, D. Manson, R. Vali, M. Khan, N. Palaniyar, D. B. Hill, D. A. Hall, C. R. Marshall,
568 M. Knowles, M. A. Zariwala, M. Kesimer, S. D. Dell, Hereditary Mucin Deficiency
569 Caused by Biallelic Loss-of-Function of MUC5B. *Am. J. Respir. Crit. Care Med.* (2022),
570 doi:10.1164/RCCM.202106-1456OC.
- 571 32. S. Gsell, E. Loiseau, U. D’Ortona, A. Viallat, J. Favier, Hydrodynamic model of
572 directional ciliary-beat organization in human airways. *Sci. Reports 2020 101*, **10**, 1–12
573 (2020).
- 574 33. E. Loiseau, S. Gsell, A. Nommick, C. Jomard, D. Gras, P. Chanez, U. D’Ortona, L.
575 Kodjabachian, J. Favier, A. Viallat, Active mucus–cilia hydrodynamic coupling drives self-
576 organization of human bronchial epithelium. *Nat. Phys.* **2020 1611**, **16**, 1158–1164 (2020).
- 577 34. W. H. Anderson, R. D. Coakley, B. Button, A. G. Henderson, K. L. Zeman, N. E. Alexis,
578 D. B. Peden, E. R. Lazarowski, C. W. Davis, S. Bailey, F. Fuller, M. Almond, B. Qaqish,
579 E. Bordonali, M. Rubinstein, W. D. Bennett, M. Kesimer, R. C. Boucher, The relationship
580 of mucus concentration (hydration) to mucus osmotic pressure and transport in chronic
581 bronchitis. *Am. J. Respir. Crit. Care Med.* **192**, 182–190 (2015).

- 582 35. L. A. Hancock, C. E. Hennessy, G. M. Solomon, E. Dobrinskikh, A. Estrella, N. Hara, D.
583 B. Hill, W. J. Kissner, M. R. Markovetz, D. E. Grove Villalon, M. E. Voss, G. J. Tearney,
584 K. S. Carroll, Y. Shi, M. I. Schwarz, W. R. Thelin, S. M. Rowe, I. V. Yang, C. M. Evans,
585 D. A. Schwartz, Muc5b overexpression causes mucociliary dysfunction and enhances lung
586 fibrosis in mice. *Nat. Commun.* **9**, 1–10 (2018).
- 587 36. C. Ehre, Z. L. Rushton, B. Wang, L. N. Hothem, C. B. Morrison, N. C. Fontana, M. R.
588 Markovetz, M. F. Delion, T. Kato, D. Villalon, W. R. Thelin, C. R. Esther, D. B. Hill, B. R.
589 Grubb, A. Livraghi-Butrico, S. H. Donaldson, R. C. Boucher, An improved inhaled
590 mucolytic to treat airway muco-obstructive diseases. *Am. J. Respir. Crit. Care Med.* **199**,
591 171–180 (2019).
- 592 37. K. Joyner, D. Song, R. F. Hawkins, R. D. Silcott, G. A. Duncan, A rational approach to
593 form disulfide linked mucin hydrogels. *Soft Matter* (2019), doi:10.1039/C9SM01715A.
- 594 38. B. S. Schuster, L. M. Ensign, D. B. Allan, J. S. Suk, J. Hanes, Particle tracking in drug and
595 gene delivery research: State-of-the-art applications and methods. *Adv. Drug Deliv. Rev.* **91**
596 (2015), pp. 70–91.
- 597 39. T. B. Gagliardi, M. E. Goldstein, D. Song, K. M. Gray, J. W. Jung, M. A. Ignacio, K. M.
598 Stroka, G. A. Duncan, M. A. Scull, Rhinovirus C replication is associated with the
599 endoplasmic reticulum and triggers cytopathic effects in an in vitro model of human airway
600 epithelium. *PLOS Pathog.* **18**, e1010159 (2022).
- 601 40. M. Woodall, B. Reidel, M. Kesimer, R. Tarran, D. L. Baines, Culture with apically applied
602 healthy or disease sputum alters the airway surface liquid proteome and ion transport
603 across human bronchial epithelial cells. *Am. J. Physiol. Cell Physiol.* **321** (2021),
604 doi:10.1152/AJPCELL.00234.2021.
605

606 Acknowledgments

607 We acknowledge the BioWorkshop core facility in the Fischell Department of
608 Bioengineering at the University of Maryland – College Park for use of their dynamic light
609 scattering instrument, microplate reader, and rheometer.
610

611 Funding:

612 Burroughs Wellcome Fund Career Award at the Scientific Interface (GAD)
613 Cystic Fibrosis Foundation grant DUNCAN18I0 (GAD, MAS)
614 National Institutes of Health grant R21AI142050 (MAS, GAD)
615 National Institutes of Health grant R01HL151840 (MAS)
616 National Institutes of Health grant T32AI125186A (EI, LK)
617

618 Author contributions:

619 Conceptualization: DS, MAS, GAD
620 Methodology: DS, EI, MAS, GAD
621 Investigation: DS, EI
622 Visualization: DS, LK
623 Supervision: MAS, GAD
624 Writing—original draft: DS
625 Writing—review & editing: DS, EI, MAS, GAD
626

627 **Competing interests:** Authors declare that they have no competing interests.
628

629 **Data and materials availability:** All data are available in the main text or the
630 supplementary materials.
631